

Supplementary Information

Ammonium Ionic Liquid Cation Promotes Electrochemical CO₂ Reduction to Ethylene over Formate while Inhibiting the Hydrogen Evolution on Copper Electrode

*Ashok Kumar Ummireddi,^ψ Shilendra Kumar Sharma,[‡] and Raj Ganesh S. Pala^{*ψ‡}*

^ψDepartment of Chemical Engineering, Indian Institute of Technology Kanpur, 208016, India

[‡]Materials Science Programme, Indian Institute of Technology Kanpur, 208016, India

*Corresponding Author: rpala@iitk.ac.in

EXPERIMENTAL SECTION

1.1 Chemicals and Materials

Potassium bicarbonate ($\geq 99.95\%$, Lot # MKBW2890V), Ace gas dispersion tube with porous fritted glass tip (O.D. 7 mm, porosity 25-50 μm (C), product # Z507660) were purchased from Sigma Aldrich; glassy carbon plate (2 mm, type 2, Lot # Q12D013), Graphite rods (product # 40766, 6.15 mm dia. x 102 mm long, 99.9995% (metals basis)), and copper foil (0.25 mm, 99.9999% Lot # W15C026) were purchased from Alfa Aesar; nitric acid (69%), and ortho-phosphoric acid (85%) were purchased from Merck; Anion exchange membrane (Selemion AMV-N) was purchased from AGC Inc.; leak-free (Ag/AgCl) reference electrode (LF-1.6-100, 1.6 mm O.D., 100 mm barrel) was purchased from Innovative Instruments, Inc.; potassium ferricyanide (99%) was purchased from Thermo Fisher Scientific; Polyether ether ketone (PEEK) sheets, tubes, and nuts were purchased from Shree Krishna Polymers, India; All

calibration gas mixtures were obtained from Chemtron Science Laboratories Pvt. Ltd., India; CO₂ (99.999%), Ar (99.999%), H₂ (99.999%), Air (99.999%) and N₂ (99.999%) were purchased from Sigma Gases and Services, India and used as received; Ethylene propylene diene monomer (EPDM) O-rings were purchased from Polymax India; Teflon O-rings (square and rectangular in shape) were made at the institute workshop from a sheet of Teflon. Milli-Q water (18.2 MΩ-cm) was used to prepare electrolytes. All the chemicals were used without further purification. 1-bromobutane (99%, Lot # STBD3815V), sodium tetrafluoroborate (98%, Lot # S55135-508), 1-butyl-1-methylpyrrolidinium tetrafluoroborate (≥97%, Lot # BCBR5293V), and tetraethylammonium tetrafluoroborate (99%, Lot # BCBN6288V) were purchased from Sigma Aldrich; and 1-butyl-3-methylimidazolium tetrafluoroborate (≥98%, Lot # 10206687), was purchased from Alfa Aesar; 1-methylpyrazole (>99%, Lot # 86HLO-MQ) was purchased from TCI Chemicals; acetonitrile (≥99.9%) was purchased from Merck. Electrolytes were prepared with Milli-Q water (18.2 MΩ-cm), and all the chemicals were used as received.

1.2 Synthesis of 1-butyl-2-methylpyrazolium tetrafluoroborate ([BMPy][BF₄])

1-butyl-2-methylpyrazolium tetrafluoroborate ([BMPy⁺][BF₄⁻]) was synthesized by following a reported protocol with slight modifications.¹ 1-Bromobutane (9.18 g, 67 mmol) was added to 1-methylpyrazole (5.00 g, 60.9 mmol) in the argon atmosphere, and the reaction mixture was stirred at 80 °C for 48 h in the argon atmosphere (**Fig. S1**). After cooling, unreacted reactants were removed under reduced pressure, and the residue (1-butyl-2-methylpyrazolium bromide) was dissolved in acetonitrile (50 mL).

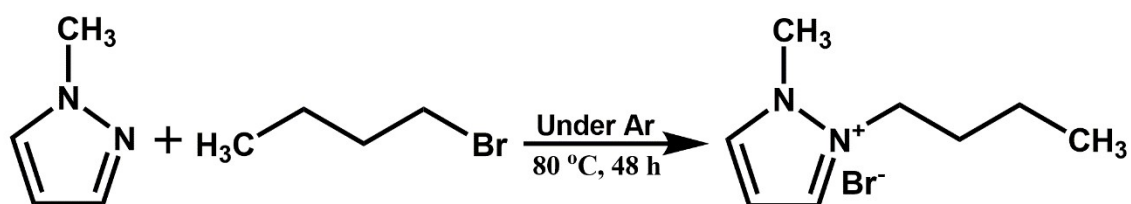


Fig. S1 Synthesis of 1-butyl-2-methylpyrazolium bromide.

Sodium tetrafluoroborate (6.70 g, 61 mmol) was added to the solution of 1-butyl-2-methylpyrazolium bromide in acetonitrile and stirred for 24 h at room temperature. The precipitate (NaBr) was separated by filtration (**Fig. S2**). Followed by the filtrate was dried under the vacuum to remove acetonitrile from the product. To further precipitate NaBr from the product, the product was dissolved in a mixture of dichloromethane and ethanol (1:1 v/v). The precipitate was separated by filtration. The filtrate was dried under a vacuum to remove the solvent from the product—a pale yellowish liquid with a 59% yield (8.12 g).

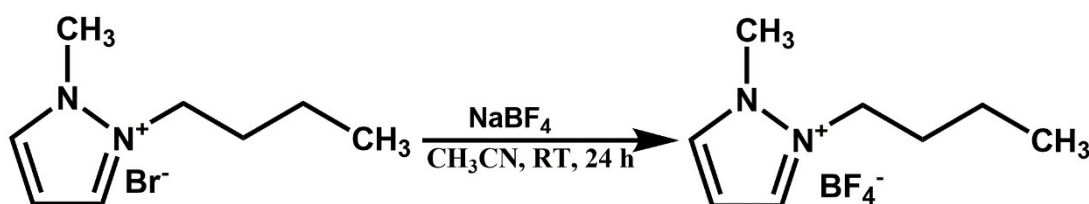


Fig. S2 Synthesis of 1-butyl-2-methylpyrazolium tetrafluoroborate.

1.3 ¹H NMR of 1-butyl-2-methylpyrazolium tetrafluoroborate ([BMPyra][BF₄])

¹H NMR (500 MHz, chloroform-d, δ): 8.12 (d, 1H, Pz H, J = 2.0 Hz), 8.03 (d, 1H, Pz H, J = 3.0 Hz), 6.60 (t, 1H, Pz H, J = 3.0 Hz), 4.38 (t, 2H, CH₂, J = 7.5 Hz), 4.09 (s, 3H, CH₃), 1.79 (p, 2H, CH₂, J = 8.5 Hz), 1.34 (sx, 2H, CH₂, J = 8.0 Hz), 0.89 (t, 3H, CH₃, J = 7.5 Hz). (**Fig. S3**)

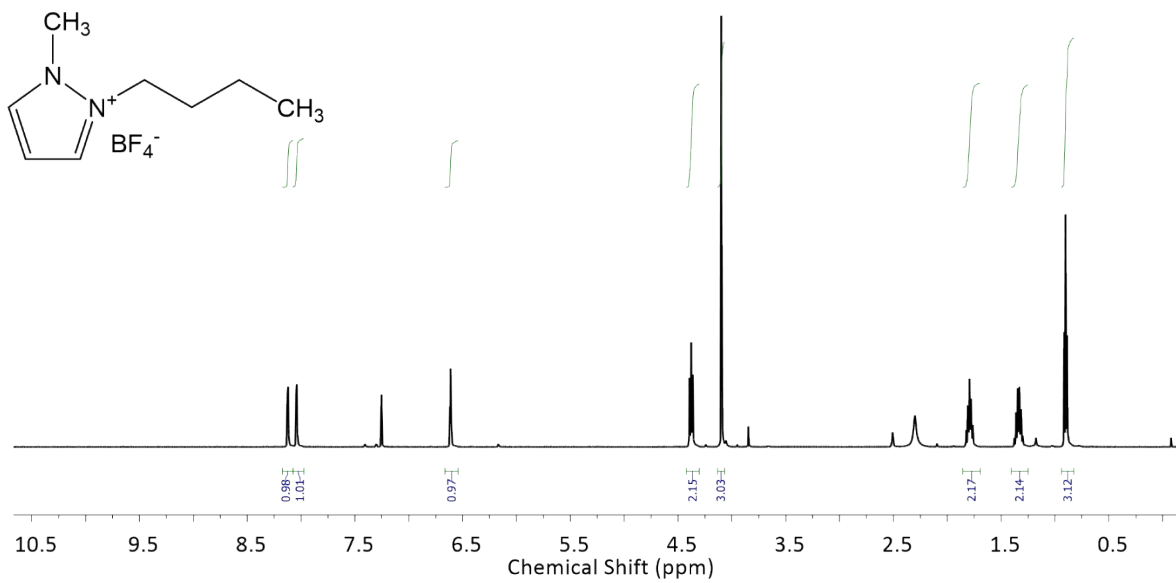


Fig. S3 ¹H NMR spectra of 1-butyl-2-methylpyrazolium tetrafluoroborate (chloroform-d).

Table S1 Bader charges on the atoms of 1-butyl-2-methylpyrazolium cation.

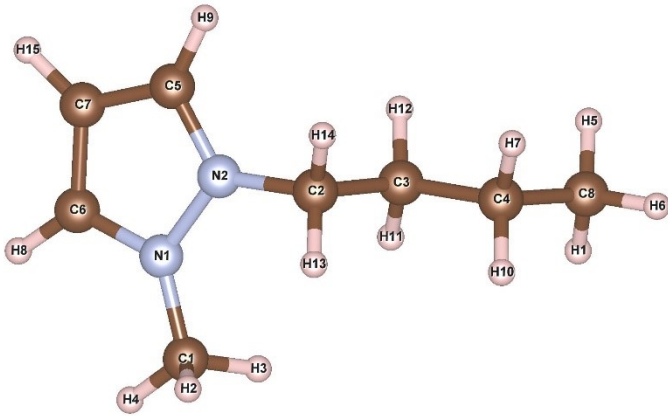
Structure of 1-Butyl-2-methylpyrazolium (BMPyra ⁺) cation	Label of the atom	Bader Charge on the atom (e)
	C1	0.19
	C2	0.26
	C3	-0.05
	C4	-0.04
	C5	0.37
	C6	0.39
	C7	-0.04
	C8	-0.14
	H1	0.04
	H2	0.15
	H3	0.10
	H4	0.15
	H5	0.06
	H6	0.11
	H7	0.05
	H8	0.20
	H9	0.21
	H10	0.05
	H11	0.04
	H12	0.08
H13	0.11	
H14	0.09	
H15	0.19	
N1	-0.76	
N2	-0.74	

Table S2 Bader charges on the atoms of tetraethylammonium cation.

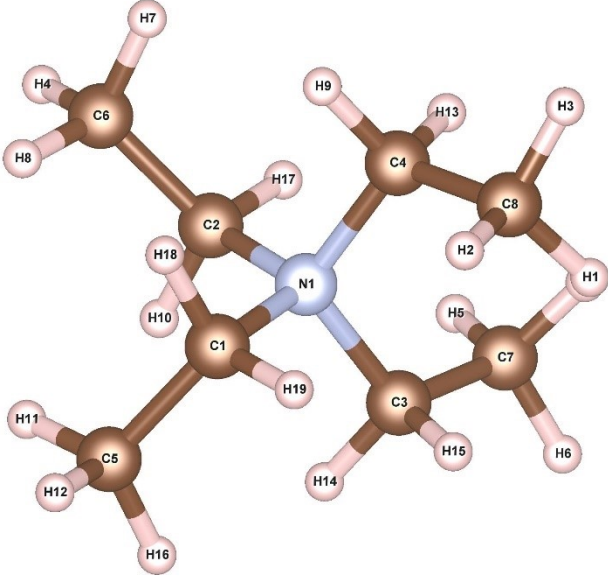
Structure of Tetraethylammonium (TEA ⁺) cation	Label of the atom	Bader Charge on the atom (e)
	C1	0.15
	C2	0.15
	C3	0.15
	C4	0.15
	C5	-0.14
	C6	-0.14
	C7	-0.14
	C8	-0.14
	H1	0.08
	H2	0.08
	H3	0.11
	H4	0.11
	H5	0.08
	H6	0.11
	H7	0.08
	H8	0.08
	H9	0.08
	H10	0.11
	H11	0.09
	H12	0.11
	H13	0.11
H14	0.08	
H15	0.11	
H16	0.08	
H17	0.08	
H18	0.11	
H19	0.08	
H20	0.09	
N1	-0.83	

Table S3 Bader charges on the atoms of 1-butyl-1-methylpyrrolidinium cation.

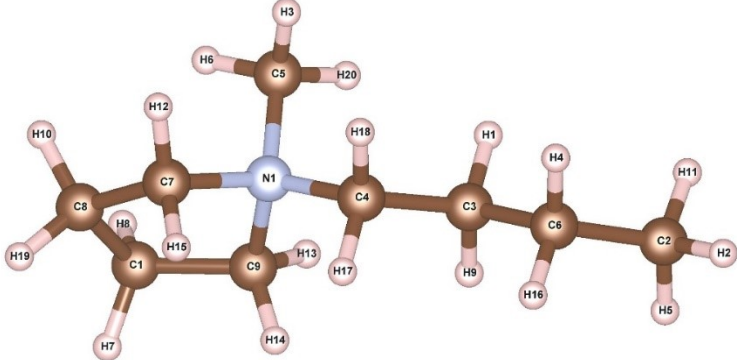
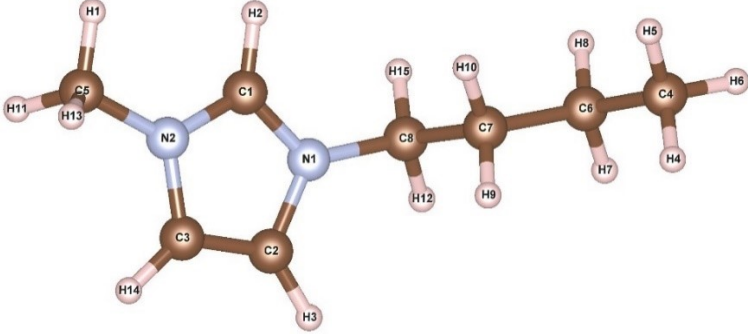
Structure of 1-Butyl-1-methylpyrrolidinium (BMPyrro ⁺) cation	Label of the atom	Bader Charge on the atom (e)
	C1	-0.01
	C2	-0.12
	C3	0.00
	C4	0.17
	C5	0.11
	C6	-0.01
	C7	0.19
	C8	-0.07
	C9	0.18
	H1	0.02
	H2	0.09
	H3	0.12
	H4	0.05
	H5	0.02
	H6	0.11
	H7	0.08
	H8	0.07
	H9	0.05
	H10	0.10
	H11	0.08
	H12	0.10
H13	0.10	
H14	0.07	
H15	0.08	
H16	0.01	
H17	0.09	
H18	0.09	
H19	0.08	
H20	0.13	
N1	-0.91	

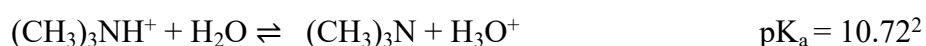
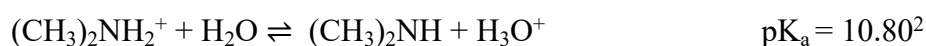
Table S4 Bader charges on the atoms of 1-Butyl-3-methylimidazolium cation.

Structure of 1-Butyl-3-methylimidazolium (BMIm ⁺) cation	Label of the atom	Bader Charge on the atom (e)
	C1	0.93
	C2	0.32
	C3	0.35
	C4	-0.13
	C5	0.23
	C6	0.02
	C7	-0.05
	C8	0.21
	H1	0.08
	H2	0.21
	H3	0.23
	H4	0.05
	H5	0.07
	H6	0.06
	H7	0.03
	H8	0.03
	H9	0.07
	H10	0.06
	H11	0.13
	H12	0.11
	H13	0.12
H14	0.19	
H15	0.10	
N1	-1.15	
N2	-1.19	

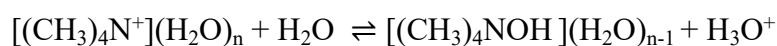
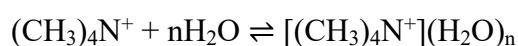
1.4 Estimation of pK_a values of ionic liquid cations

pK_a of hydrated cations used in this study is not available in the literature. Since each ionic liquid cation is synthesized by alkylation of the corresponding precursor, we assume that the pK_a of hydrated ionic liquid cation is directly proportional to its precursor's pK_a. Based on this analysis, we assumed that the pK_a value of an alkylated molecule does not change much from its precursor after each alkylation step.

For instance, in the case of ethylamine,



pK_a is not changed much after each alkylation step. For tetraethylammonium



Based on this analysis, we assume a relationship between the pK_a of hydrated ionic liquid cation and its precursor's pK_a. Moreover, pK_a of hydrated ionic liquid cation is directly proportional/follows the same trend as its precursor's pK_a.

Table S5 pK_a values of precursors used to synthesize ionic liquid cations.

Ionic Liquid Cation	Precursor for Ionic Liquid Cation	pK_a of precursor
TEA ⁺	Triethylammonium	10.72 ²
BMPyrro ⁺	1-methyl pyrrolidine	10.46 ²
BMIm ⁺	1-methyl imidazole	7.20 ³
BMPyra ⁺	1-methyl pyrazole	2.09 ³

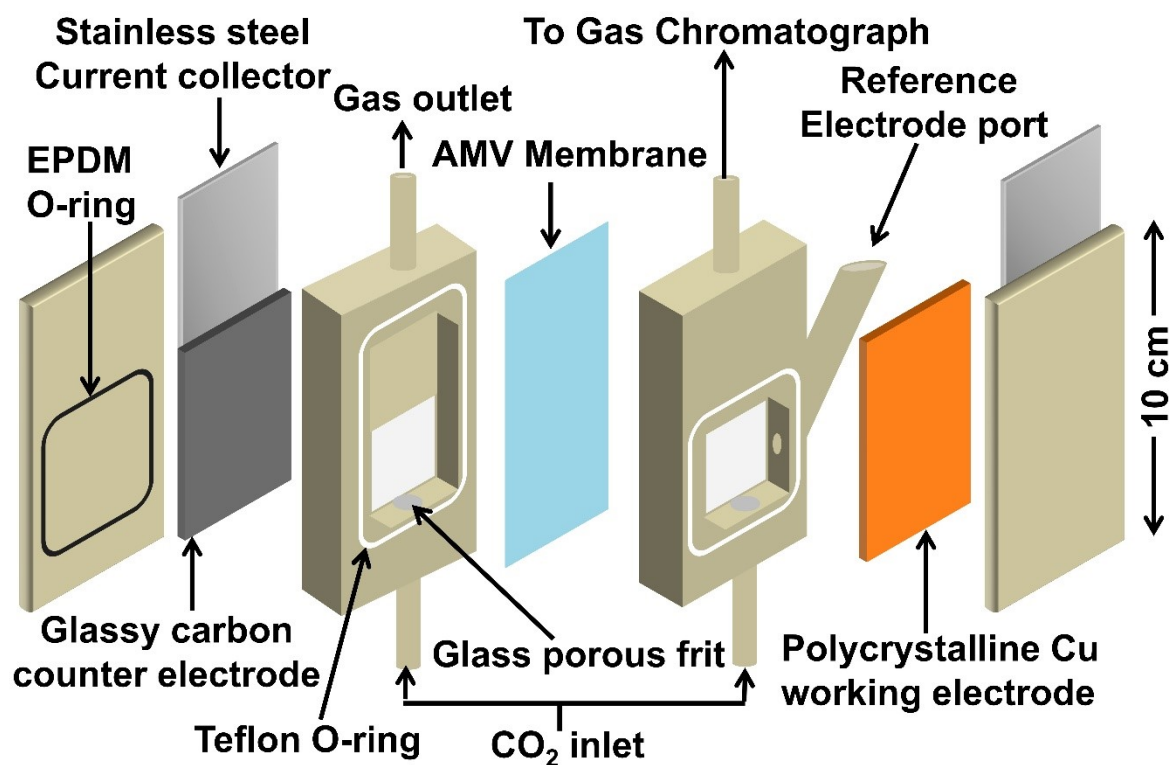


Fig. S4 The schematic of the electrochemical cell used for electrochemical CO₂ reduction reactions. Redrawn from ref no.⁴

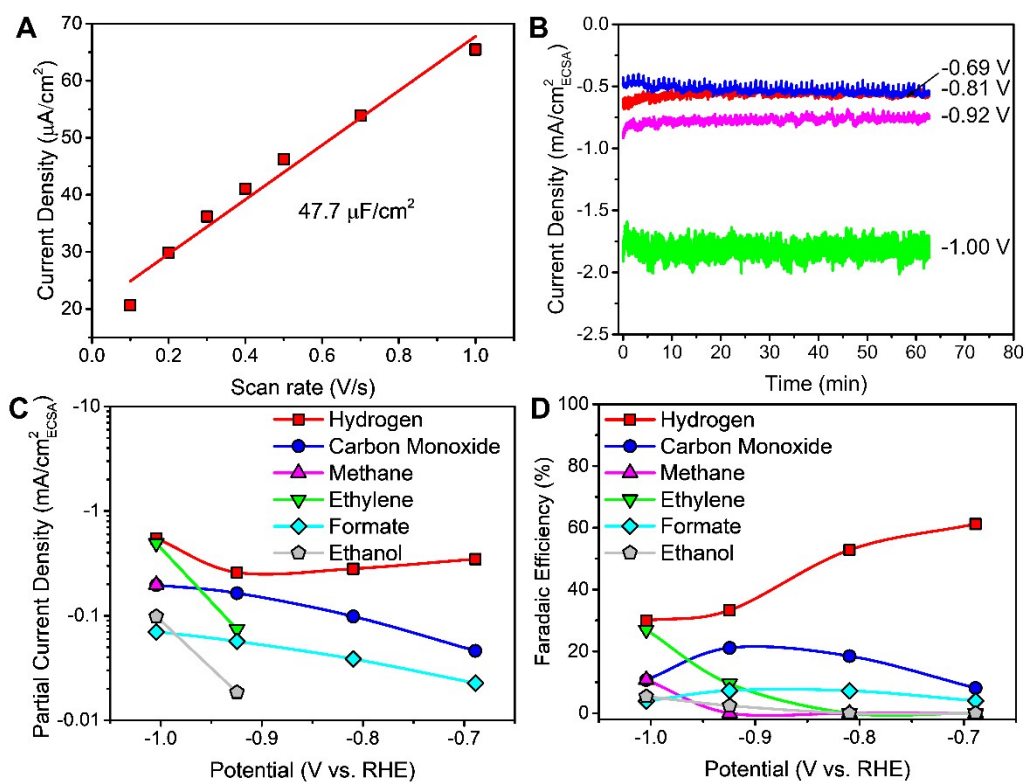


Fig. S5 The plots of (A) ECSA measurement, (B) chronoamperometry measurement at different potentials, (C) partial current densities, and (D) Faradaic efficiencies of different products at different potentials on the copper electrode in the presence of $1 \text{ mM } [\text{TEA}^+]\text{BF}_4^-$ in 0.1 M KHCO_3 .

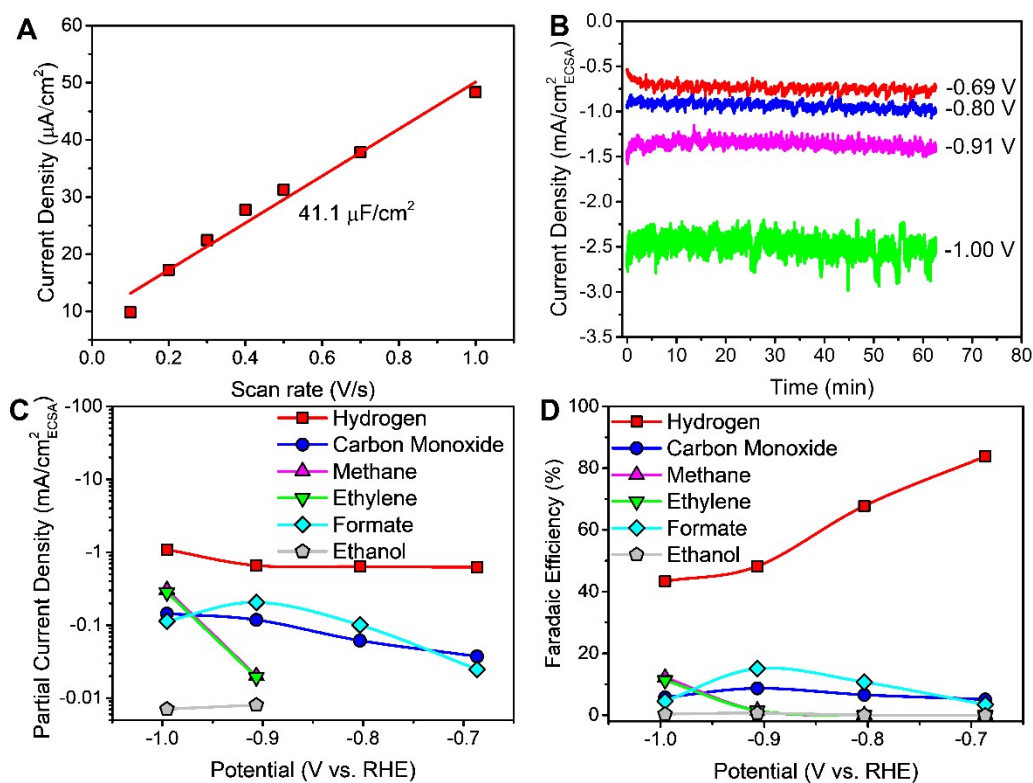


Fig. S6 The plots of (A) ECSA measurement, (B) chronoamperometry measurement at different potentials, (C) partial current densities, and (D) Faradaic efficiencies of different products at different potentials on the copper electrode in the presence of 1 mM $[\text{BMIm}^+]\text{BF}_4^-$ in 0.1 M KHCO_3 .

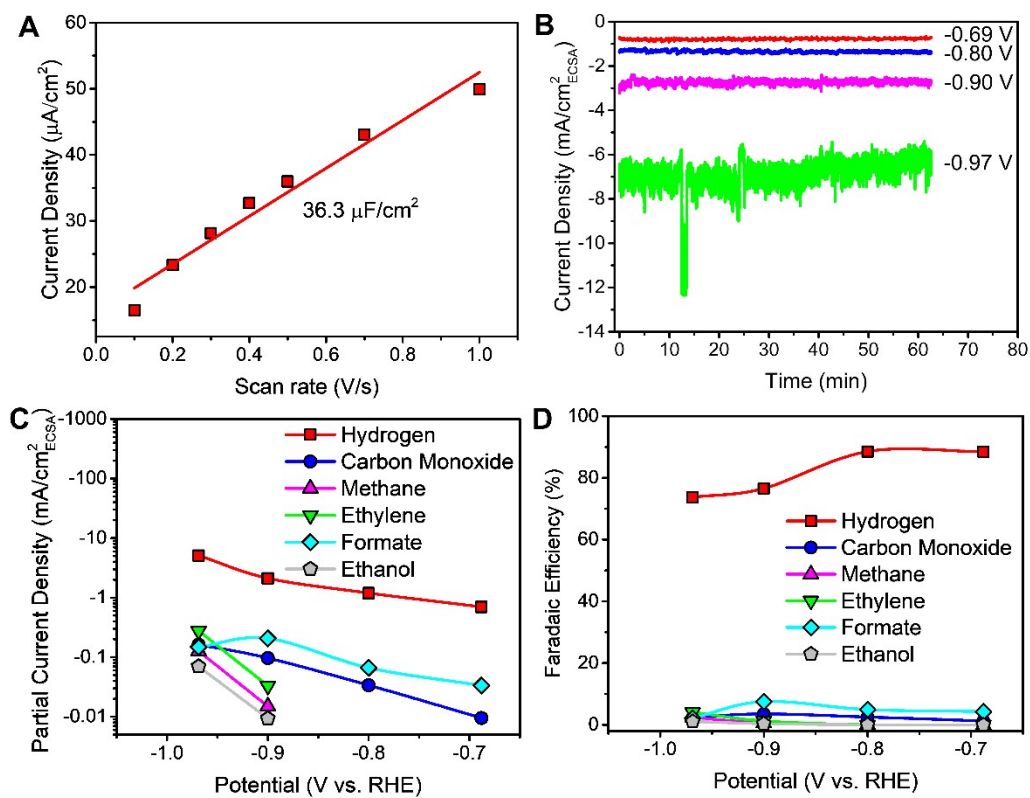


Fig. S7 The plots of (A) ECSA measurement, (B) chronoamperometry measurement at different potentials, (C) partial current densities, and (D) Faradaic efficiencies of different products at different potentials on the copper electrode in the presence of $1 \text{ mM } [\text{BMPyra}^+]\text{BF}_4^-$ in 0.1 M KHCO_3 .

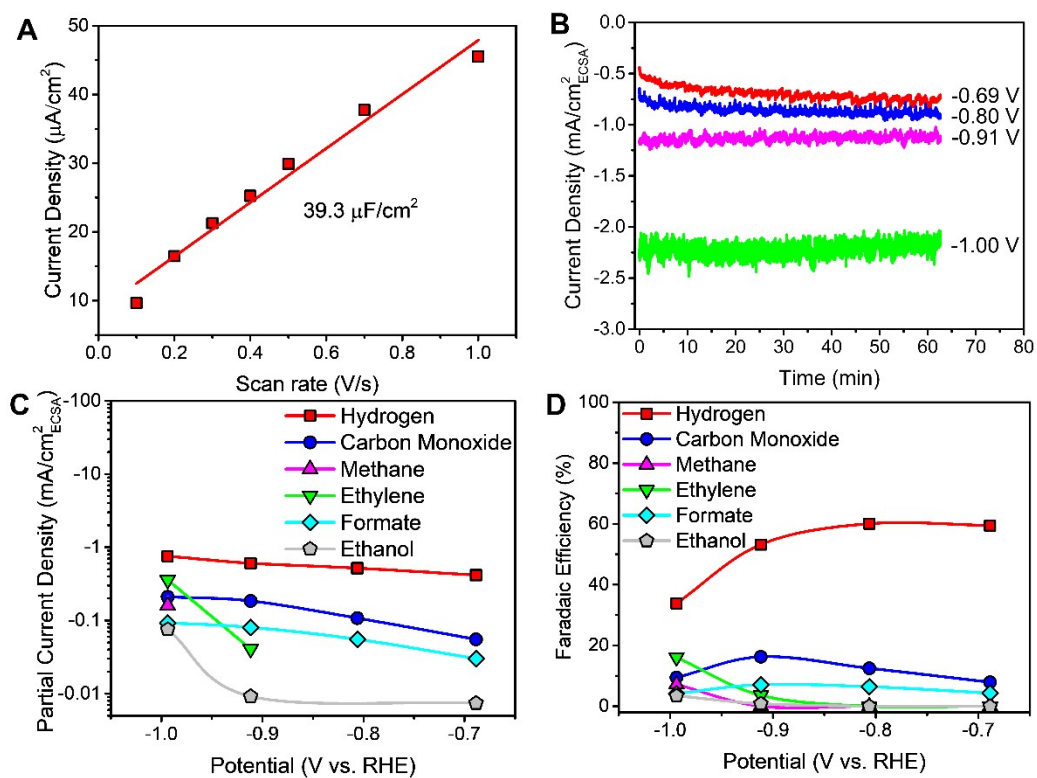


Fig. S8 The plots of (A) ECSA measurement, (B) chronoamperometry measurement at different potentials, (C) partial current densities, and (D) Faradaic efficiencies of different products at different potentials on the copper electrode in the presence of 1 mM [BMPyrro⁺]BF₄⁻ in 0.1 M KHCO₃.

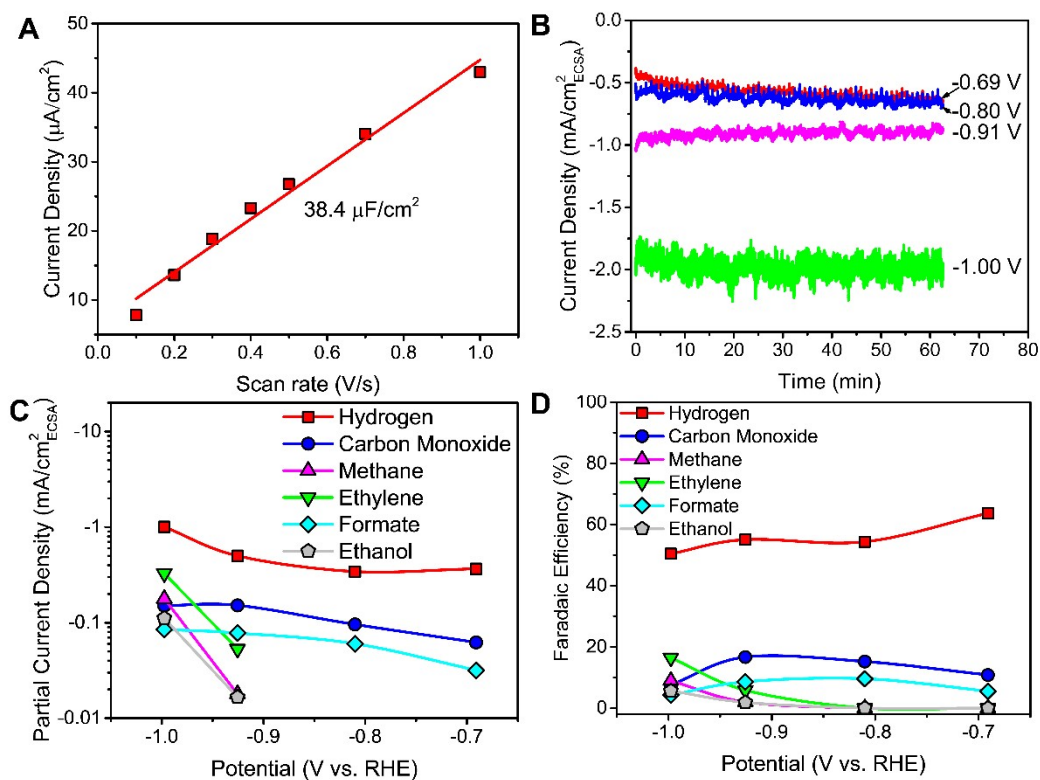


Fig. S9 The plots of (A) ECSA measurement, (B) chronoamperometry measurement at different potentials, (C) partial current densities, and (D) Faradaic efficiencies of different products at different potentials on the copper electrode in the absence of ionic liquid.

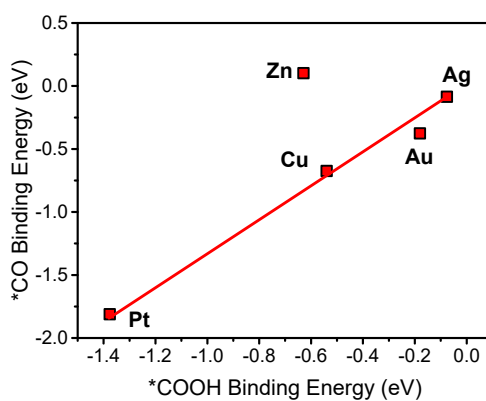


Fig. S10 Correlation of *COOH and *CO binding energies on different metal surfaces.

Redrawn from ref no.^{5, 6}

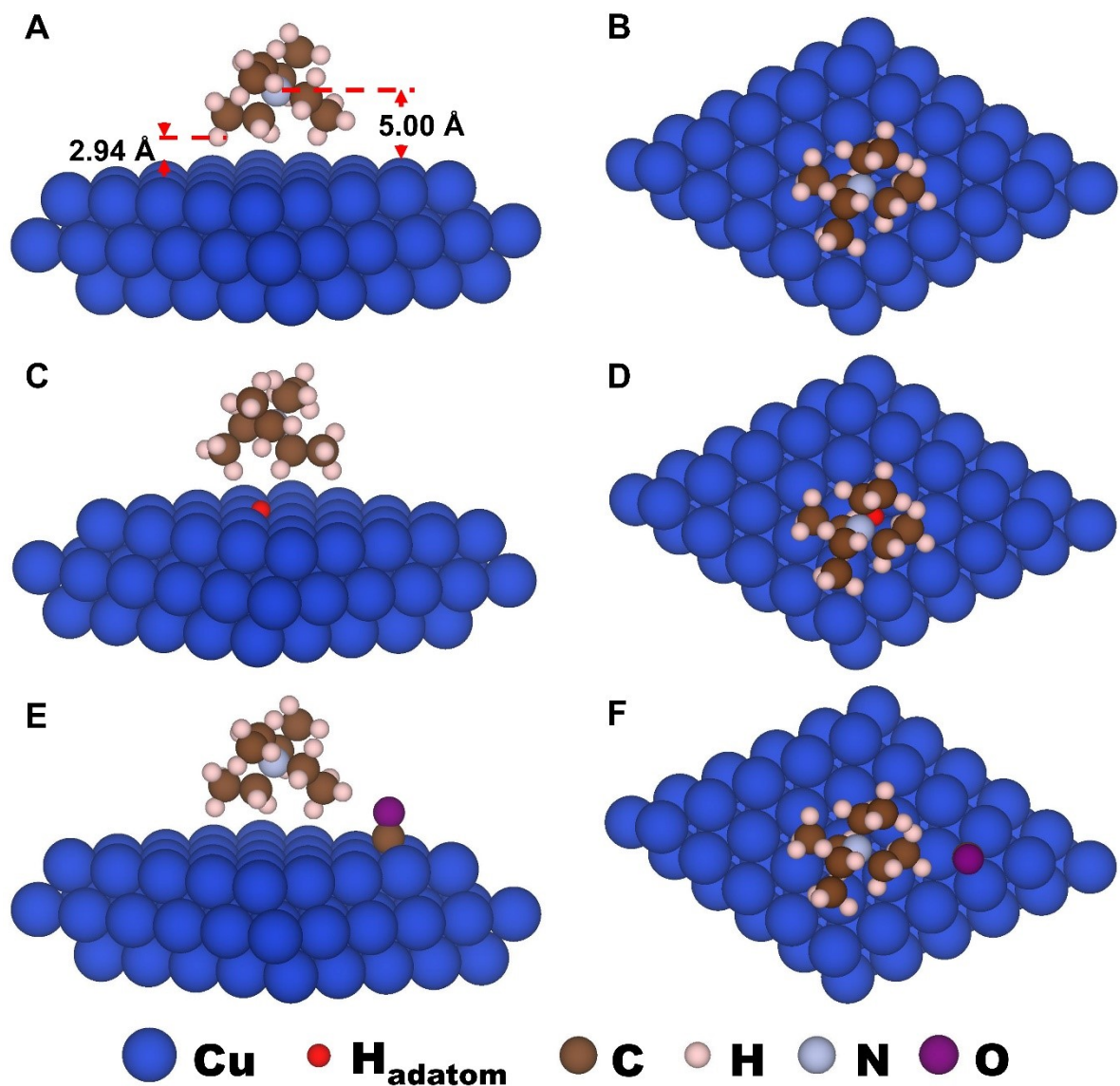


Fig. S11 Optimized geometries of (A) side and (B) top view of tetraethylammonium cation adsorbed, (C) side and (D) top view of tetraethylammonium cation adsorbed along with H adatom, and (E) side and (F) top view of tetraethylammonium cation adsorbed along with CO molecule on Cu(111) surface.

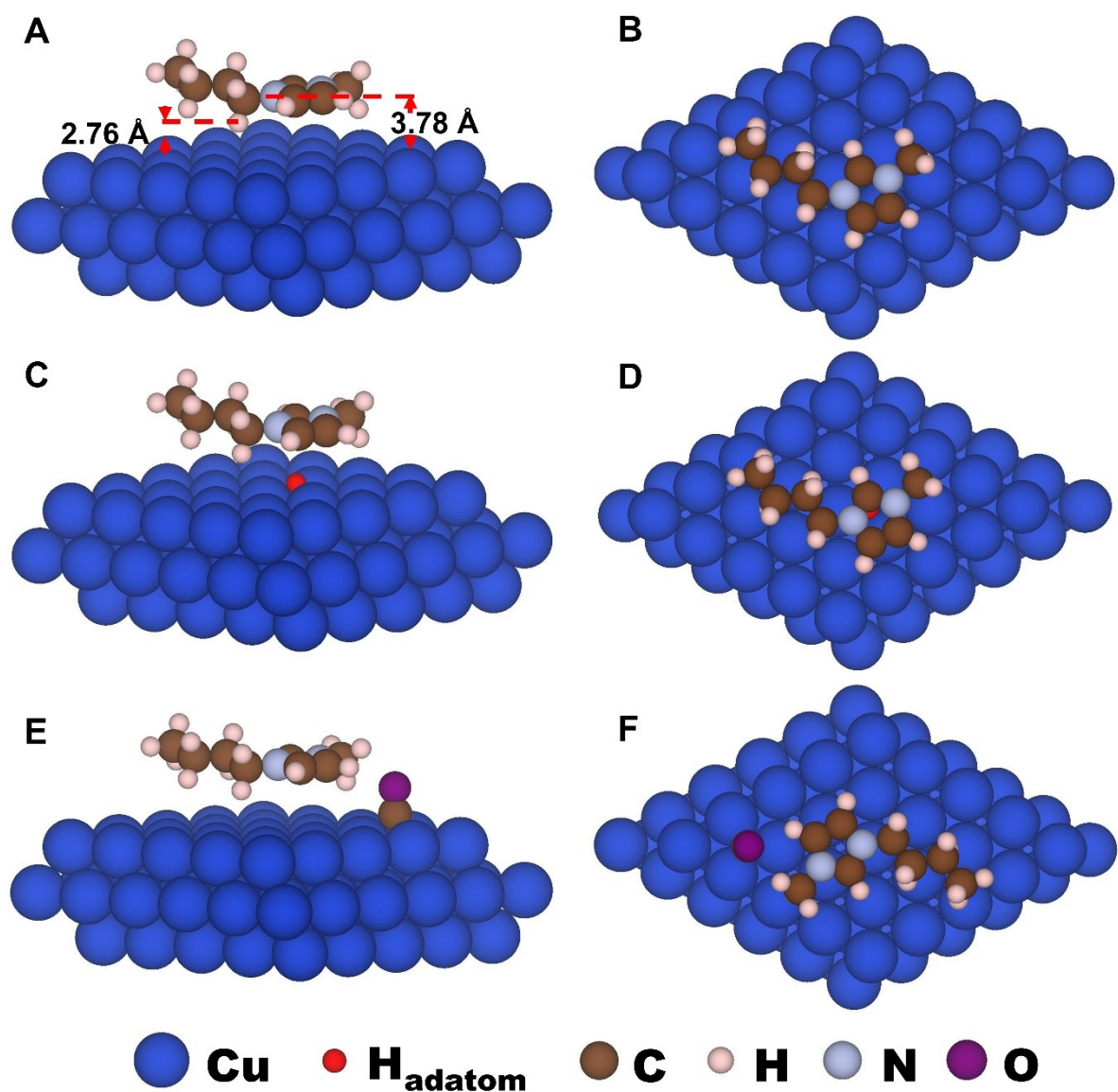


Fig. S12 Optimized geometries of (A) side and (B) top view of 1-butyl-3-methylimidazolium cation adsorbed, (C) side and (D) top view of 1-butyl-3-methylimidazolium cation adsorbed along with H adatom, and (E) side and (F) top view of 1-butyl-3-methylimidazolium cation adsorbed along with CO molecule on Cu(111) surface.

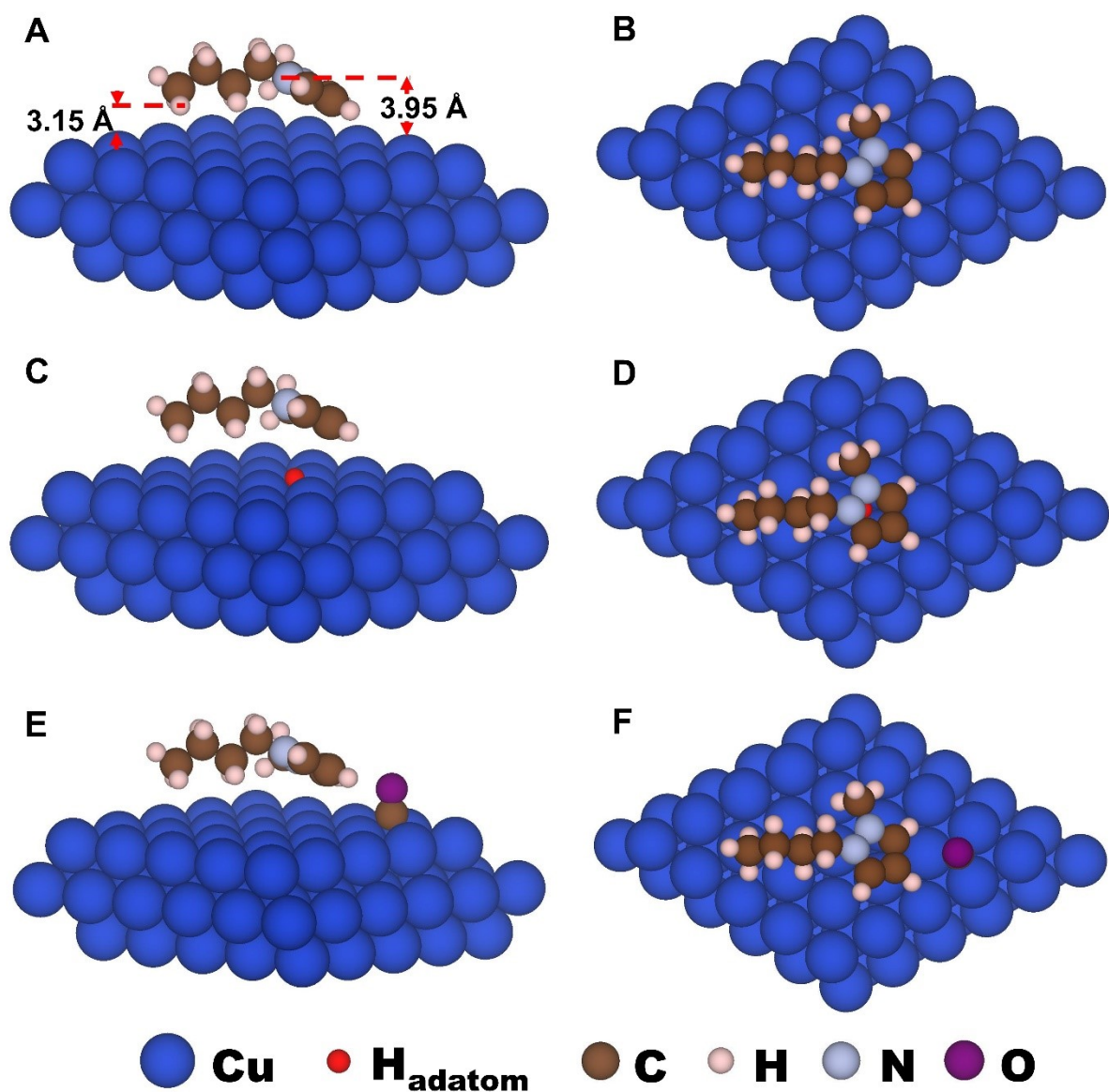


Fig. S13 Optimized geometries of (A) side and (B) top view of 1-butyl-2-methylpyrazolium cation adsorbed, (C) side and (D) top view of 1-butyl-2-methylpyrazolium cation adsorbed along with H adatom, and (E) side and (F) top view of 1-butyl-2-methylpyrazolium cation adsorbed along with CO molecule on Cu(111) surface.

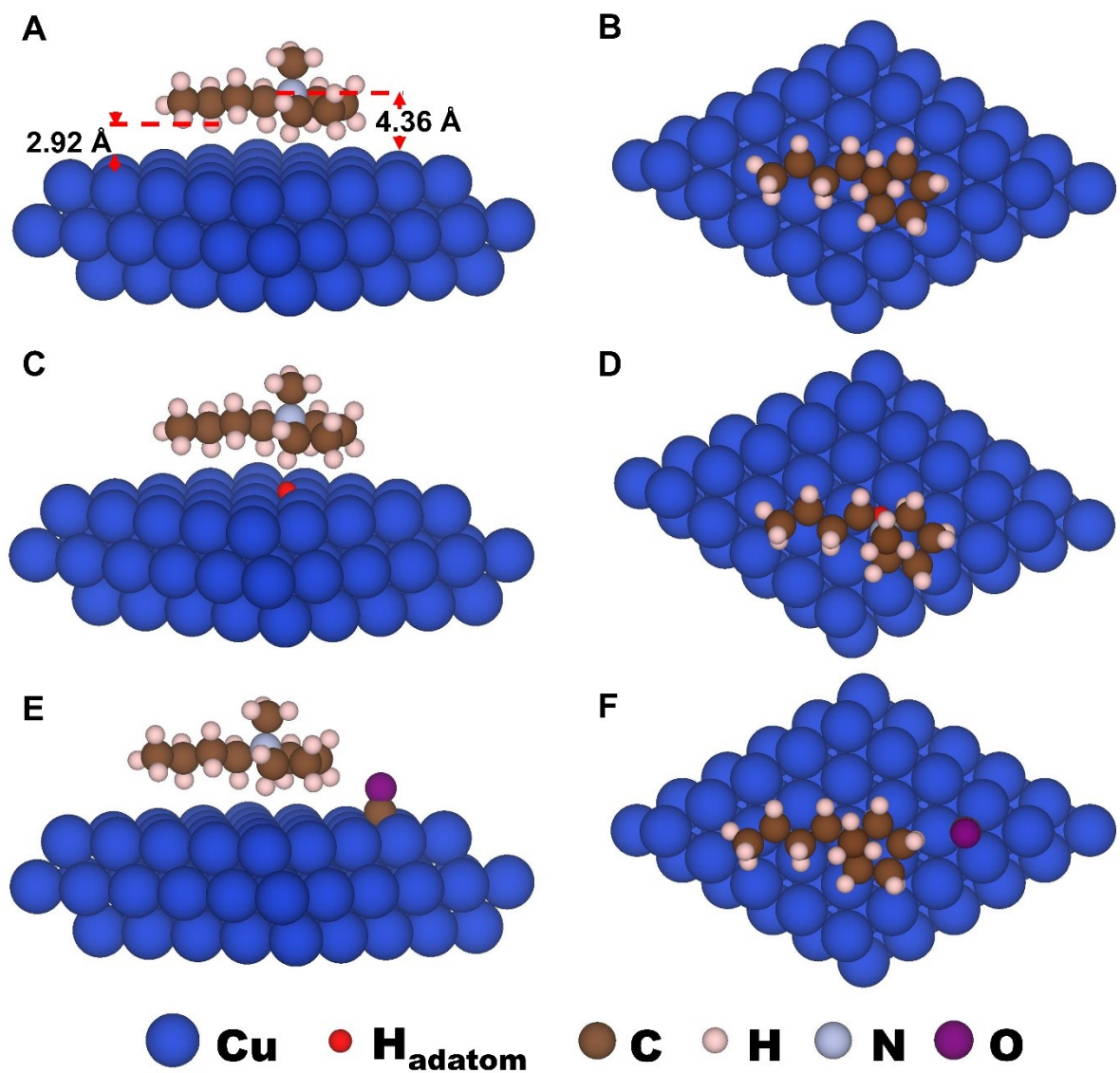


Fig. S14 Optimized geometries of (A) side and (B) top view of 1-butyl-1-methylpyrrolidinium cation adsorbed, (C) side and (D) top view of 1-butyl-1-methylpyrrolidinium cation adsorbed along with H adatom, and (E) side and (F) top view of 1-butyl-1-methylpyrrolidinium cation adsorbed along with CO molecule on Cu(111) surface.

References

1. D. Vasilyev, E. Shirzadi, A. V. Rudnev, P. Broekmann and P. Dyson, *ACS Appl. Energy Mater.*, 2018, **1**, 5124-5128.
2. J. A. Dean, *Lange's handbook of chemistry*, McGraw-Hill New York, 1992.
3. J. Catalán and J. Elguero, *J. Chem. Soc., Perkin Trans. 2*, 1983, DOI: 10.1039/P29830001869, 1869-1874.
4. A. K. Ummireddi, S. K. Sharma and R. G. S. Pala, *Catal. Sci. Technol.*, 2021, **11**, 4857-4865.
5. K. P. Kuhl, T. Hatsukade, E. R. Cave, D. N. Abram, J. Kibsgaard and T. F. Jaramillo, *J. Am. Chem. Soc.*, 2014, **136**, 14107-14113.
6. J. T. Feaster, C. Shi, E. R. Cave, T. Hatsukade, D. N. Abram, K. P. Kuhl, C. Hahn, J. K. Nørskov and T. F. Jaramillo, *ACS Catal.*, 2017, **7**, 4822-4827.